Hindawi
Geofluids
Volume 2021, Article ID 8147366, 13 pages
https://doi.org/10.1155/2021/8147366

Research Article

Optimization of the Plastic Area of a Borehole Based on the Gas Extraction Effect and Its Engineering Application

Kuan Wu,[1,2] Shiliang Shi,[1] Yi Lu,[1] He Li,[1] and Min Li[1]

[1]*Hunan University of Science and Technology, School of Resource, Environment and Safety Engineering, Xiangtan, Hunan 411201, China*
[2]*Hunan University of Science and Technology, Work Safety Key Lab on Prevention and Control of Gas and Roof Disasters for Southern Coal Mines, Xiangtan, Hunan 411201, China*

Correspondence should be addressed to Shiliang Shi; sslhnust@yeah.net

Received 22 July 2021; Accepted 15 October 2021; Published 11 November 2021

Academic Editor: Bo Tan

Gas extraction is most commonly used to control gas disasters in coal mines. The distribution of the plastic zone around a borehole and the sealing quality are key factors affecting gas extraction. In this paper, the plastic zone was simulated by COMSOL, and a theoretical equation of the plastic zone radius was derived. In addition, an antispray hole equipment and the "two plugging and one injection" sealing technology were proposed. The results show that a larger borehole pore size corresponds to a larger plastic zone and larger range of pressure relief of the borehole. The error between the calculated and simulated plastic zone radii is within 1%, and the modified equation is applicable to Puxi mine. The loss and harm caused by borehole spraying are reduced by applying antispray hole equipment. By applying the "two plugging and one injection" sealing technology and phosphogypsum-based self-produced gas expansion paste material to block the borehole, the sealing quality is improved and an accurate gas mixing flow, pure flow, and concentration were obtained. As the plastic zone enlarges, the gas extraction flow gradually increases with, but the relative variation of flow first increases and subsequently decreases. Considering the safety and economy of construction, the optimal radius of the plastic zone is 64.9 mm.

1. Introduction

Coal is a type of energy used throughout the world, and it is widely used in the power, fuel, and oil industries [1–4]. However, with the continuous depletion of shallow coal reserves and the increasing demand for coal, coal mine disasters gradually increase with the increase of the mining depth [5–8]. Among coal mine disasters, gas disasters are considered the most serious threat to the safety of China's coal industry [9–13]. Over the past 70 years, there have been 25 catastrophic coal mine accidents, which have killed more than 100 people in China, and 18 of these accidents were gas disasters [14, 15]. Therefore, to prevent coal and gas outburst in the coal mining process, gas drainage, high-pressure water injection hydraulic fracturing, mine ventilation dilution gas, protective coal mining, and other technical measures are usually adopted in coal mines, among which gas drainage is the most commonly used method [16–19]. In some high-gas-content mines in South China, drilling through the layer is often performed to control gas disasters [20–22].

One of the main factors affecting the effect of gas drainage is the borehole diameter [23–25]. Once a borehole is formed, the coal body around the borehole undergoes pressure relief and plastic damage, forming plastic zone for gas migration [26–29]. At present, based on the elastic-plastic theory, Guo et al. [30] studied the stress distribution characteristics and pressure relief range of coal around the borehole by analysing the borehole stress and air leakage form. Cheng et al. [31] established the mechanical model of borehole softening and expansion based on the Hoek Brown criterion and deduced the elastic area, plastic softening area, and fracture around the borehole. Su [32] used theoretical analysis and numerical simulation to analyse the failure mechanism of the coal body in a bedding hole, which formed the elastic deformation area around the hole. The stress distribution and displacement equation of the coal

body in the plastic softening zone and the pressure relief fracture zone were analysed.

Another main factor that affects the effect of gas drainage is the sealing quality of the borehole [33, 34]. In recent years, many new sealing methods and sealing materials have been proposed by a number of scholars. Zhang et al. [35, 36] developed the "strong-weak-strong" borehole sealing technology, which can improve the CMM drainage efficiency of a single high-gas low-permeability coal seam. Liu et al. [37] tested 10 groups of sealing materials and presented a new sealing method and an appropriate sealing equipment, including an automatic grout pump and two types of rubber bottom subs, which were used to improve the sealing performance of inclined cross-measure drainage boreholes. Zhou et al. [38] proposed a second-sealing-plugging technology for gas drainage and examined the migration law of gas movement in the fracture network of the coal seam. Ni et al. [39] studied the microcharacteristics of borehole sealing materials composed of frozen composite material with PU and expansive cement. Xiang et al. [40] developed a flexible gel sealing material and experimentally compared its sealing performance with that of conventional sealing materials. Ge et al. [41] conceived a novel hydraulic fracturing sealing material composed of cement, hardening, accelerating, and water-reducing admixtures; polypropylene fibre; and mixing water. Despite the emergence of new technologies and materials for antiair leakage, these methods increase the drainage efficiency on the premise of a long sealing depth, which increases the construction difficulty and cost of sealing boreholes. An economical and effective sealing method with a short sealing depth for inseam boreholes is necessary to prolong the efficient continuous drainage time and increase the drainage amount of methane [42–45].

In this paper, based on the elastic-plastic theory, the COMSOL simulation software was used to simulate the plastic area range of the coal body around a drill hole and verify whether the plastic area ranges of the theory and simulation were consistent with each other and analysed the relationship between different borehole diameters and plastic area ranges. The new type of blowout preventer was used to construct a test drilling hole, the "two plugging and one injection" sealing technology and phosphogypsum-based self-produced gas expansion slurry material were used to block the drilling hole, and the accurate gas mixed flow, pure flow, and concentration data were measured. Finally, the appropriate plastic area of the borehole was determined by analysing the gas drainage effect in different plastic areas of the drilling hole.

2. General Situation of Puxi Mine

Jiahe Mining Co., Ltd. is the raw coal company of Hunan Heijin Times Co., Ltd., and the subordinate Puxi mine is a gas outburst mine in the northeast of Jiahe County, Chenzhou, Hunan Province, as shown in Figure 1. The administrative area is under the jurisdiction of Xinglang town, Jiahe County. The geographical coordinates of the mining area are 112° 24′ 52″~112° 27′ 11″ E and 25° 35′ 10″~25° 39′ 41″ N. The north-south strike of the mine is 4.5 km; the east-west strike is 1.8 km, on average; the area is 8.6186 km^2. There are seven coal seams in the mine: coal seam II, coal seam III, coal seam IV, coal seam V, coal seam V_2, coal seam VI, and coal seam VII from top to bottom. Coal seam V has a stable occurrence and is the main coal seam of the mine, while coal seams II and VI are locally minable coal seams. The average thickness and inclination angle of coal seam V are 2.42 m and 25°, respectively. Since the mine was put into operation, coal and gas outburst have occurred 106 times, and the types of outburst are mainly extrusion and pour-out. The maximum coal outburst amount is 430 t, and the maximum gas outburst amount is 46,000 m^3. With the increase in mining depth, the outburst frequency and intensity are increasing. Although many projects have been performed in the borehole through the coal seam via the floor roadway in the mine, the borehole, which has a diameter of 65 mm, is not ideal. The extraction time is long, the extraction concentration is low, and regional outburst elimination cost is relatively high. Therefore, it is very important to determine the appropriate borehole diameter and plastic zone range.

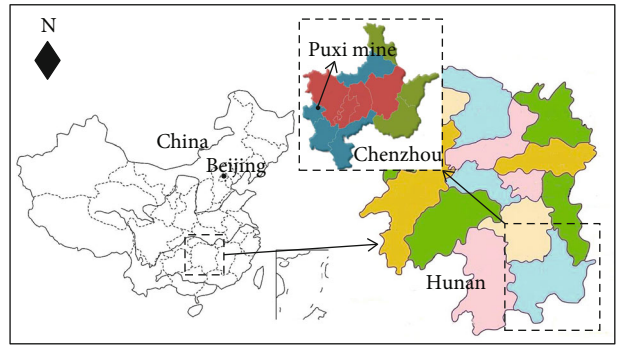

Figure 1: Location of Puxi mine.

3. Numerical Simulation of the Plastic Zone around the Borehole

3.1. Model and Calculation Parameters. In this paper, COMSOL Multiphysics was used to simulate and study the plastic zone in the coal body around crossing boreholes with different pore sizes. Model size selection depends on the range of the effects of stress changes around the borehole. According to theoretical analysis, a local change of the coal body only has a significant impact over a limited range, and stress changes are negligible far from the local construction site. According to the characteristics of 2254 working surfaces in Puxi mine, the model was established. Because of the symmetry of the model, only half of the computational domain was used to achieve a numerical solution. A 2 m × 2 m model is established, as shown in Figure 2. The borehole is located at the centre of the left boundary of the model. The bottom boundary of the model is fixed, that is, the vertical displacement is 0, the left boundary is symmetric constraint, and the right boundary is horizontal constraint,

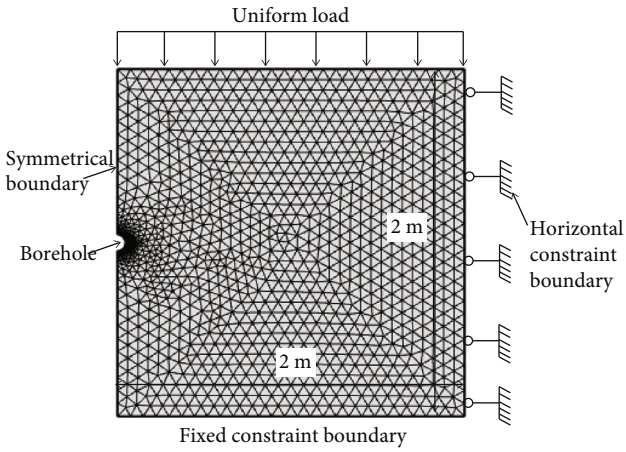

Figure 2: Geometric model.

that is, the horizontal displacement of the right boundary is 0, and the top boundary has a uniform load of 1.3 MPa to simulate the dead weight boundary of the overlying rock mass. The basic parameters of the coal seam are shown in Table 1.

3.2. Analysis of the Numerical Simulation Results. After completion of the borehole, the stress field around the borehole will change and redistribute. The coal body will expand, deform, and flow towards the borehole, causing plastic failure of the coal body. During borehole formation, the coal body adjacent to the borehole gradually bears the supported pressure of the coal body. The coal body adjacent to the borehole shows a state of stress concentration, which damages the coal body in the adjacent region because the strength is lower than the concentrated stress and forms a plastic zone.

As shown in Figure 3, after completion of the borehole, the plastic zone, elastic zone, and initial stress zone were successively formed around the borehole from inside to outside. Because the coal around the borehole was difficult to bear a large stress, the peak value of concentrated stress shifted away from the borehole wall, and the stress borne by the coal around the borehole gradually decreased and finally lowered than the original stress, which was the process of pressure relief. When the stress of the coal body at a certain distance from the borehole is lower than the strength of the coal body and only causes an elastic change but not a plastic change of the coal body, the pressure does not decrease in this area. Therefore, the range of the plastic zone, which can be expressed according the radius of the plastic zone, will affect the range of pressure relief of the borehole.

Figure 4 shows the distribution of the plastic zone around boreholes of 75 mm, 87 mm, 94 mm, 105 mm, and 113 mm from left to right. With the increased of the borehole pore size, the plastic zone around the borehole gradually increased. As shown in Figure 3, when the coal body entered the plastic state, the maximum tangential stress shifted from the periphery of the borehole to the junction of the elastic zone and plastic zone. As it extended into the coal body, the tangential stress gradually returned to the initial stress, so the peak point of tangential stress and the point of zero effective plastic strain were on the boundary of the plastic zone.

Table 1: Basic parameters of the coal seam.

No.	Model parameter	Parameter values
1	Elasticity modulus (MPa)	1180
2	Bulk modulus (MPa)	630
3	Cohesion (MPa)	0.68
4	Internal friction angle (°)	20.7
5	Tensile strength (MPa)	0.2
6	Density (kg·m^{-3})	1350

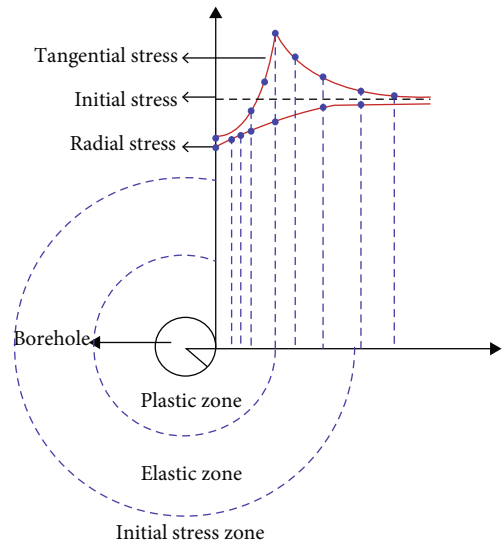

Figure 3: Stress distribution law around the borehole.

As shown in Figures 5 and 6, the tangential stress around the borehole first increased and subsequently decreased, while the effective plastic strain of the coal around the borehole gradually decreased with increasing distance from the borehole centre. Therefore, the x-coordinate that corresponds to the tangential stress peak point and the point where the effective plastic strain became 0 defined the radius of the plastic zone.

As shown in Table 2, the radii of the plastic zones of boreholes with pore sizes of 75 mm, 87 mm, 94 mm, 105 mm, and 113 mm are 46.3 mm, 53.9 mm, 57.6 mm, 65.0 mm, and 70.3 mm, respectively. Thus, a larger pore size corresponds to a larger plastic zone and larger range of pressure relief. From the perspective of gas extraction, a larger borehole diameter corresponds to a larger range of pressure relief of the coal body and a better gas extraction effect.

4. Modified Model of the Plastic Zone Range

4.1. Basic Model of Plastic Zone Range. Before analysing the plastic zone of the borehole, we can assume some conditions to transform the stress distribution around the borehole into a round hole problem of plane strain: (1) the surrounding

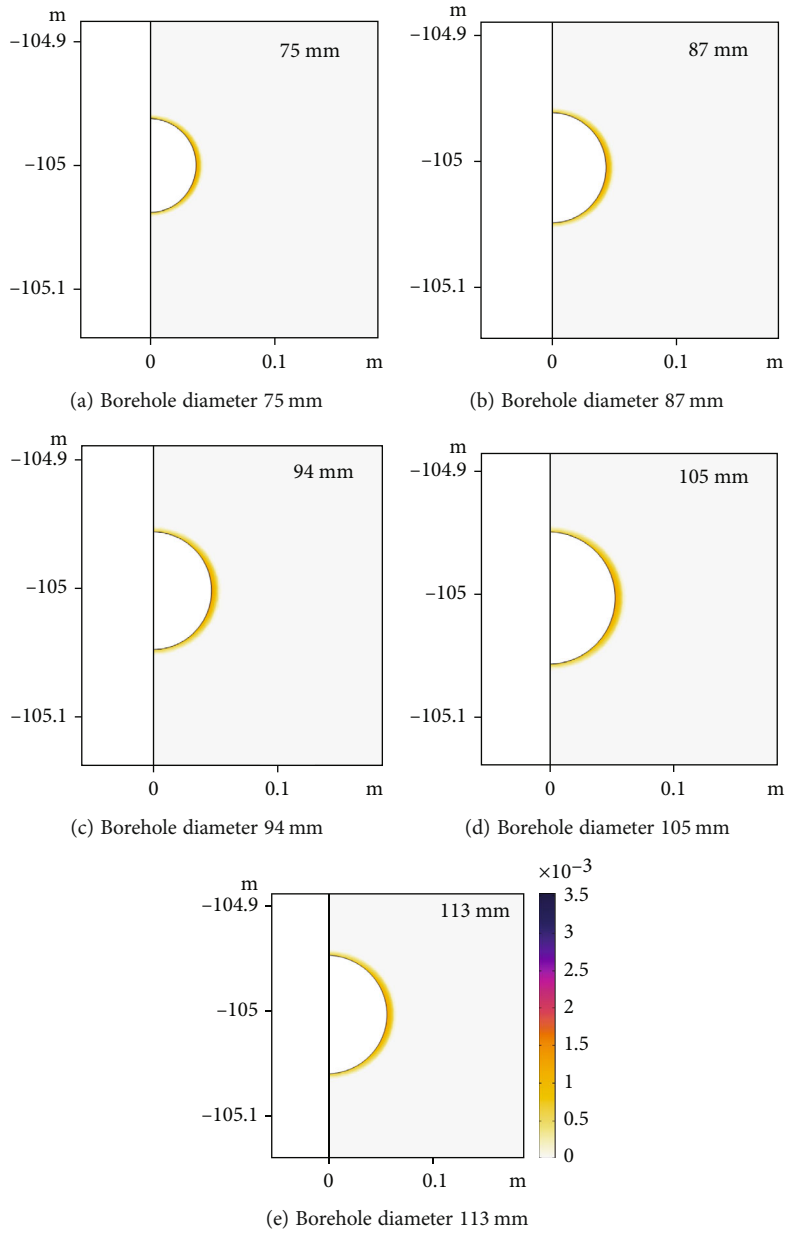

Figure 4: Plastic zone of different pore sizes.

rock mass of the borehole is a homogeneous, continuous, and isotropic ideal elastic-plastic body; (2) the properties of coal in different directions are identical; (3) after the borehole forms, the transverse and longitudinal displacement and deformation are small; (4) the lateral pressure coefficient of the surrounding rock is 1.

A plane coordinate system is established with the centre of the borehole as the origin. The distance between any point of the plane and the centre of the borehole is r. If the radius of plastic zone is R_p, the variation gradient of cohesion in the plastic zone can be expressed as Equation (1).

$$j_c = \frac{c_0 - c_s}{R_p - R}, \tag{1}$$

where j_c is the gradient of change; c_0 is the initial cohesion, MPa; c_s is the residual cohesion, MPa; R_p is the radius of plastic zone, m; and R is the borehole radius, m. In the plastic zone, the cohesion at distance r from the drilling centre can be expressed as Equation ($_2$).

$$c^* = c_s + j_c(r - R). \tag{2}$$

In the elastic zone, $c^* = c_0$. For axisymmetric problems, the stress satisfies the equilibrium equation, so Equation (3) can be obtained.

$$\frac{d\sigma}{dr} + \frac{\sigma_r - \sigma_\theta}{r} = 0, \tag{3}$$

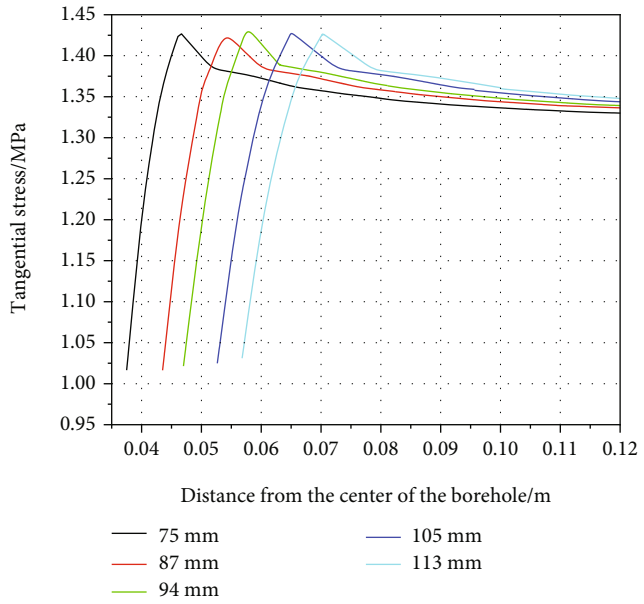

FIGURE 5: Tangential stress distribution of different pore sizes.

where σ_r is the radial stress, MPa, and σ_θ is the tangential stress, MPa. In the plastic zone, the rock mass material satisfies the equilibrium equation and the corresponding yield criterion. Hence, in this paper, the Mohr-Coulomb criterion, which is currently the most widely used criterion, is still used. In polar coordinates, the Mohr-Coulomb criterion can be expressed as Equation (4).

$$\sigma_\theta = \xi\sigma_r + \frac{2c^* \cos\varphi}{1-\sin\varphi}, \tag{4}$$

where $\xi = 1 + \sin\varphi/1 - \sin\varphi$; φ is the internal friction angle of coal, °.

4.1.1. Stress in the Plastic Zone. Substitute Equation (4) into Equation (3) to obtain Equation (5).

$$\frac{d\sigma_r}{dr} + \frac{(1-\xi)}{r}\sigma_r = \frac{\sigma^*}{r}, \tag{5}$$

where $\sigma^* = 2c^* \cos\varphi/1 - \sin\varphi$. Using the differential formula, Equation (6) is obtained.

$$\sigma_r = e^{-\int 1-\xi/rdr}\left(\int \frac{\sigma^*}{r} e^{\int 1-\xi/rd} dr + C\right). \tag{6}$$

By substituting Equation (2) into Equation (6) and combining with $\xi = 1 + \sin\varphi/1 - \sin\varphi$, we obtain Equation (7).

$$\sigma_r = (j_c R - c_s)\cot\varphi + \frac{2j_c \cos\varphi}{1-3\sin\varphi} r + r^{\xi-1} C. \tag{7}$$

When r is equal to R, σ_r is equal to 0. Thus, the integral constant can be obtained by making $k_1 = (j_c R - c_s)\cot\varphi$ and $k_2 = 2j_c \cos\varphi/1 - 3\sin\varphi$ and combining the condition of the stress boundary. Therefore, Equation (8) can be obtained.

$$\sigma_r = k_1 + k_2 r - k_1\left(\frac{r}{R}\right)^{\xi-1} - k_2 r\left(\frac{r}{R}\right)^{\xi-2}. \tag{8}$$

By substituting Equation (8) into Equation ($_4$), we obtain Equation (9).

$$\sigma_\theta = \xi k_1 + \xi k_2 r - \xi k_1\left(\frac{r}{R}\right)^{\xi-1} \xi k_2 r\left(\frac{r}{R}\right)^{\xi-2} + \sigma^*. \tag{9}$$

According to the total theory of plasticity, ε_Z is equal to 0 in the problem of plane strain. Thus, the plastic constitutive Equation (10) can be obtained.

$$\left\{\begin{array}{l} \varepsilon_r = \dfrac{\psi}{4G^*}(\sigma_r - \sigma_\theta) \\ \varepsilon_\theta = \dfrac{\psi}{4G^*}(\sigma_\theta - \sigma_r) \end{array}\right\}, \tag{10}$$

where ε_r is the radial strain; ψ is the plastic index; G^* is the weakening shear modulus, MPa; and ε_θ is the tangential strain. The elastic constitutive Equation (11) is as follows:

$$\left\{\begin{array}{l} \varepsilon_r = \dfrac{1-\nu^2}{E}\left(\sigma_r - \dfrac{\nu}{1-\nu}\sigma_\theta\right) \\ \varepsilon_\theta = \dfrac{1-\nu^2}{E}\left(\sigma_\theta - \dfrac{\nu}{1-\nu}\sigma_r\right) \end{array}\right\}, \tag{11}$$

where V is Poisson's ratio; E is the modulus of elasticity, MPa. We substitute Equations (8) and (9) into Equations (10) and (11) to obtain the strain expression as Equation (12).

$$\left\{\begin{array}{l} \varepsilon_r^p = \dfrac{\psi}{4G^*}[(1-\xi)\sigma_r - \sigma^*] + \dfrac{1-\nu^2}{E}\left[\left(\dfrac{1-(1+\xi)\nu}{1-\nu}\sigma_r\right) - \dfrac{\nu}{1-\nu}\sigma^*\right] \\ \varepsilon_\theta^p = \dfrac{\psi}{4G^*}[\sigma^* - (1-\xi)\sigma_r] + \dfrac{1-\nu^2}{E}\left[\left(\xi - \dfrac{\nu}{1-\nu}\right)\sigma_r + \sigma^*\right] \end{array}\right\}, \tag{12}$$

where ε_r^p and ε_θ^p are the radial strain and tangential strain in the plastic zone, MPa, respectively.

4.1.2. Stress in the Elastic Zone. The stress solution in the elastic region can be expressed as Equation (13).

$$\left.\begin{array}{l} \sigma_r \\ \sigma_\theta \end{array}\right\} = A \pm \frac{B}{r^2}, \tag{13}$$

where A and B are undetermined coefficients.

When r approaches infinity, $\sigma_r = \sigma_\theta = p_0 = A$; when r is equal to R_p, $\sigma^* = \sigma_0 = 2c_0 \cos\varphi/1 - \sin\varphi$. Simultaneously, the elastic-plastic interface satisfies Equation (14).

$$\sigma_r + \sigma_\theta = 2p_0, \tag{14}$$

where p_0 is the initial stress, MPa.

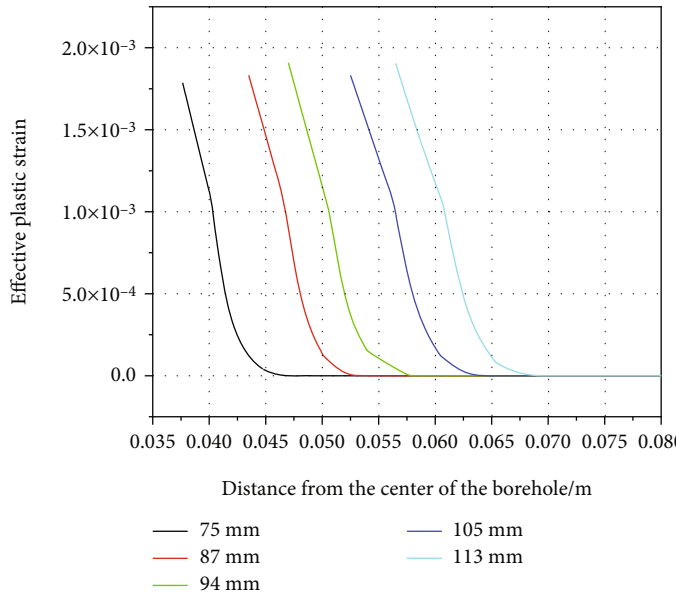

Figure 6: Effective plastic strain of different pore sizes.

Table 2: Radii of the simulated plastic zones of boreholes with different pore sizes.

Radius of borehole (mm)	37.5	43.5	47.0	52.5	56.5
Radius of plastic zone (mm)	46.3	53.9	57.6	65.0	70.3

Equation (15) can be obtained by substituting Equation (14) into Equation (3).

$$\begin{cases} \sigma_r\big|_{r=R_p} = p_0(1-\sin\varphi) - c_0\cos\varphi, \\ \sigma_\theta\big|_{r=R_p} = p_0(1+\sin\varphi) + c_0\cos\varphi. \end{cases} \tag{15}$$

Substituting Equation (15) into Equation (13), we obtain Equation (16).

$$\begin{cases} \sigma_r = p_0 - \dfrac{R_p^2}{r^2}(p_0\sin\varphi + c_0\cos\varphi), \\ \sigma_\theta = p_0 + \dfrac{R_p^2}{r^2}(p_0\sin\varphi + c_0\cos\varphi). \end{cases} \tag{16}$$

By substituting Equation (16) into Equation (11), we obtain the strain in the elastic region.

$$\begin{cases} \varepsilon_r^e = \dfrac{1+\nu}{E}\left[(1-2\nu)p_0 - (p_0\sin\varphi + c_0\cos\varphi)\dfrac{R_p^2}{r^2}\right], \\ \varepsilon_\theta^e = \dfrac{1+\nu}{E}\left[(1-2\nu)p_0 + (p_0\sin\varphi + c_0\cos\varphi)\dfrac{R_p^2}{r^2}\right] \end{cases}, \tag{17}$$

where ε_r^e and ε_θ^e are the radial strain and tangential strain in the elastic zone, MPa, respectively.

4.1.3. Radius of the Plastic Zone. At the elastoplastic interface, $r = R_p$ and $\sigma^* = 2c_0\cos\varphi/1-\sin\varphi$. Because $\sigma_r^p = \sigma_r^e$, Equation (18) can be obtained according to Equations (8) and (16).

$$k_1 + k_2R_p - k_1\left(\frac{R_p}{R}\right)^{\xi-1} - k_2r\left(\frac{R_p}{R}\right)^{\xi-2} + c_0\cos\varphi = p_0(1-\sin\varphi). \tag{18}$$

By substituting Equation (1) and the expressions of k_1 and k_2 into Equation (18), we obtain the range of the plastic zone of the borehole.

$$\begin{aligned} &\left(\frac{R_p}{R}\right)^{\xi-1}\left[(c_0-c_s)\frac{2\cos\phi}{1-3\sin\phi} + c_0\cot\phi - c_s\cot\phi\left(\frac{R_p}{R}\right)\right] \\ &+ \frac{R_p}{R}\left[p_0(1-\sin\phi) - c_0\frac{3\cos\phi(1-\sin\phi)}{1-3\sin\phi} + c_s\cot\phi\frac{1-\sin\phi}{1-3\sin\phi}\right] \\ &= p_0(1-\sin\phi) - c_0(\cos\phi - \cot\phi). \end{aligned} \tag{19}$$

In particular, when the surrounding rock of the borehole is an ideal elastoplastic body, Equation (19) can be reduced to Equation (20).

$$R_p = R\left(\frac{p_0(1-\sin\varphi) - c_0(\cos\varphi - \cot\varphi)}{c_0\cot\varphi}\right)^{1-\sin\varphi/2\sin\varphi}. \tag{20}$$

4.2. Modified Model of the Plastic Zone Range. The plastic zone radii of boreholes with different pore sizes, which were calculated by formula (20), are shown in Table 3.

Table 3: Calculated radii of the plastic zone of boreholes with different pore sizes.

Radius of borehole (mm)	37.5	43.5	47.0	52.5	56.5
Radius of plastic zone (mm)	41.9	48.6	52.5	58.6	63.1

Tables 2 and 3 show that there was an error between the numerically simulated and calculated radii of the plastic zones. Hence, formula (20) must be corrected. Figure 7 shows the variation law of the plastic zone range with the borehole radius and the variation law of the difference of the radius determined between the two methods.

As shown in Figure 7, the difference between the two methods shows an approximate first-order function with the radius as Equation (21).

$$R_1 = kR + c, \tag{21}$$

where R_1 is the difference, m; k is the slope. After calculation, the slope is 0.12, so the modified equation is shown in Equation (22).

$$R_{P1} = R_P + R_1 = R_P + 0.12R, \tag{22}$$

where R_{P1} is the modified radius of the plastic zone, m. Table 4 shows a comparison between the calculated radius of the plastic zone by Equation (22) and the simulated radius.

Table 4 shows that the error between the plastic zone radius calculated by Equation (22) and the simulated radius was within 1%, which proves that Equation (22) is applicable to Puxi mine. In Equation (22), the initial stress, cohesion, and internal friction angle are constants, so Equation (22) is a first-order function of the radius. According to Equation (22), when the radius increases, the plastic zone around the borehole also increases. The range of pressure relief of the borehole will increase, and the effect of gas extraction of the borehole will improve.

5. Analysis of the Gas Extraction Effect under Different Ranges of the Plastic Zone of the Borehole

5.1. Test Method. To study the relationship between the plastic zone of different boreholes and the gas extraction effect in Puxi mine, the effect of plastic zone radii of 46.4 mm, 53.8 mm, 58.1 mm, 64.9 mm, and 69.9 mm on the gas extraction effect was preliminarily determined and investigated, and the variations of the gas concentration, mixed flow rate, and pure flow in different plastic zones of the borehole were investigated. In principle, for the test area, we selected a newly excavated floor roadway with a length of more than 150 m, and the test site was determined to be the 2254 floor roadway in combination with the site conditions of Puxi mine.

5.2. Construction and Sealing of the Borehole

5.2.1. Application of the New Type of Antispray Hole Equipment in the Soft Coal Seam. During or after the construction of large boreholes, pulverized coal and gas are continuously ejaculated from the boreholes in a short period of time due to the soft coal quality of coal V in Puxi mine. This phenomenon is called borehole spraying. A large amount of gas emitted from the borehole over a short period of time would make the gas concentration in the tunnel abnormally increase and endanger the personal safety of underground construction personnel. To solve the problem of an abnormal increase of the gas concentration in the roadway caused by borehole spraying in the highly gassy and soft coal seam, a new type of antispray hole equipment was adopted in the test to reduce the damage caused by borehole spraying, as shown in Figure 8.

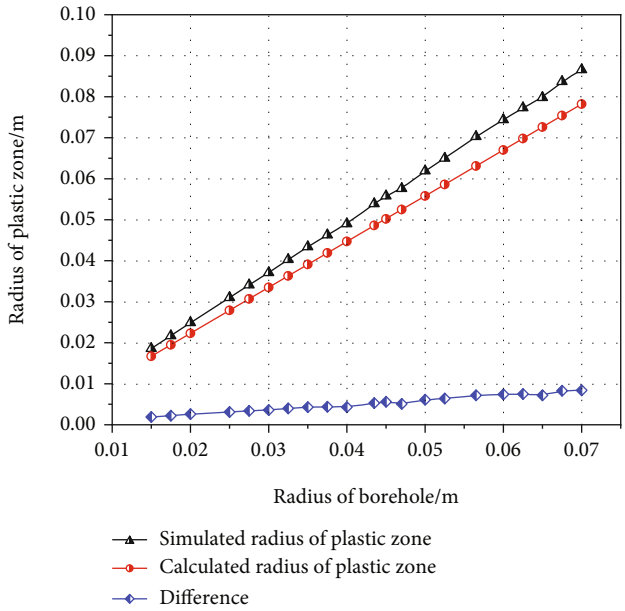

Figure 7: Comparison of the plastic zone radius.

As shown in Figure 8, the equipment is composed of an upper cylinder and a lower semicircle arc plate. In the borehole construction process, if borehole spraying occurs, the gas extraction pump will be immediately opened. When pulverized coal and gas pass through the antispray hole equipment, gas enters the gas chamber through the pumping air hole under the effect of negative pressure and subsequently enters the gas extraction pump through the short extraction pipe. The pulverized coal loses kinetic energy and flows out from the space between the upper cylinder and the lower semicircle arc plate. In the usage process, the gas concentration can be monitored by the gas concentration monitor to determine whether borehole spraying has stopped. Compared with the existing equipment, the new type of antispray hole equipment has simple structure and convenient installation and disassembly. It can effectively reduce the gas concentration when the borehole spraying. At the same time, it can separate the pulverized coal and gas twice to ensure the gas drainage effect and finally ensure the safety of personnel in the roadway. Application of this new type of antispray hole equipment solved the problem that the gas concentration in the roadway abnormally

Table 4: Comparison of the radius of the plastic zone.

Radius of borehole (mm)	37.5	43.5	47.0	52.5	56.5
The simulated radius of plastic zone (mm)	46.3	53.9	57.6	65.0	70.3
The calculated radius of plastic zone (mm)	46.4	53.8	58.1	64.9	69.9
Error (%)	0.2	0.19	0.87	0.15	0.57

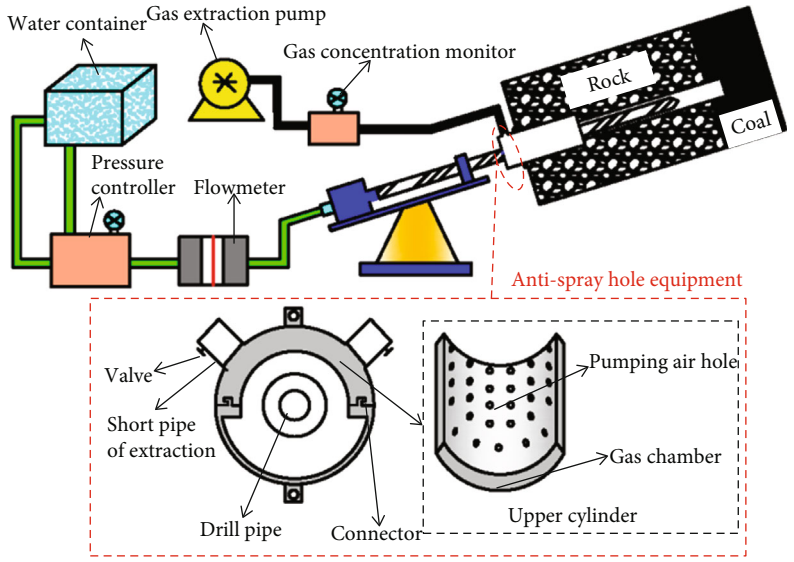

Figure 8: New type of antispray hole equipment.

increases due to gas gushing in the borehole construction process.

5.2.2. Borehole Sealing. The quality of borehole sealing directly affects the effect of gas extraction in the coal seam. By selecting the appropriate borehole sealing technology and materials, the quality of borehole sealing and the effect of gas extraction can be improved in the coal seam. Therefore, after borehole construction was completed, the "two blocks and one injection" sealing technology was selected for borehole sealing (see Figure 9). The process of grouting and hole sealing is depicted in Figure 10, a grouting pipe was used to inject phosphogypsum-based self-produced gas expansion paste material into the bag, and friction was generated between the bag and the borehole wall after the bag expanded. Under the continuous action of the grouting pump, the slurry would fill the cracks around the borehole wall to prevent gas from flowing out of the cracks.

The phosphogypsum-based self-produced gas expansion paste material is composed of the following components: 55 parts of phosphogypsum, 30 parts of water, 9 parts of cement, 0.18 parts of polyoxyethylene alkylamine, 0.9 parts of hydroxyethyl cellulose, 0.22 parts of acrylic acid, 0.39 parts of sodium methanesulfonate, 0.01 parts of ammonia persulfate, 4.0 parts of sodium bicarbonate, and 0.3 parts of microsilica powder. The preparation method is to add polyoxyethylene alkylamine and acrylic acid in water and stir to form a mixture. Then, cement, hydroxyethyl cellulose, ammonia persulfate, sodium methyl propylene sulfonate,

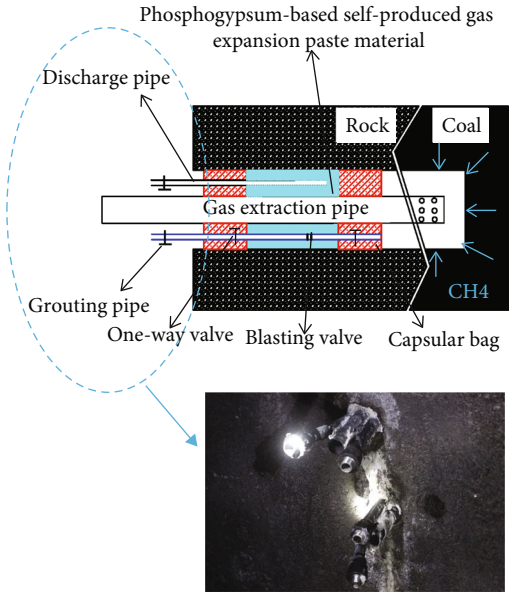

Figure 9: Principle of the "two blocks and one injection" sealing technology.

microsilica powder, and sodium bicarbonate are added to phosphogypsum to form mixed powder. Finally, the mixed powder is added to the mixture and stirred to make an expanded slurry. The phosphogypsum-based self-produced gas expansion paste material reacts slowly at room

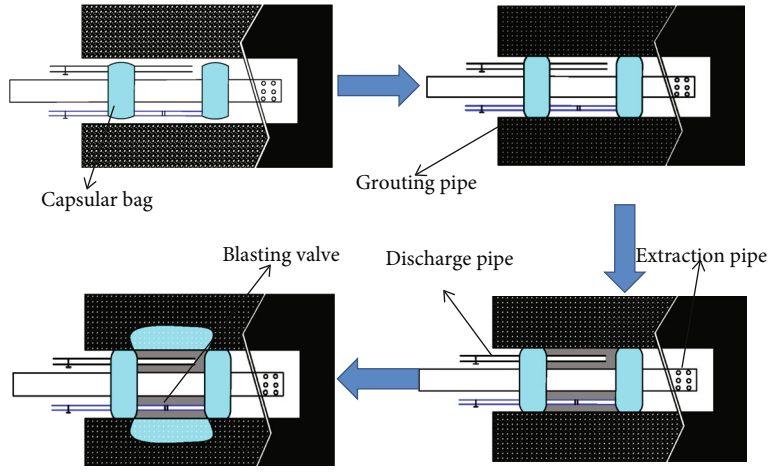

Figure 10: Hole-sealing process.

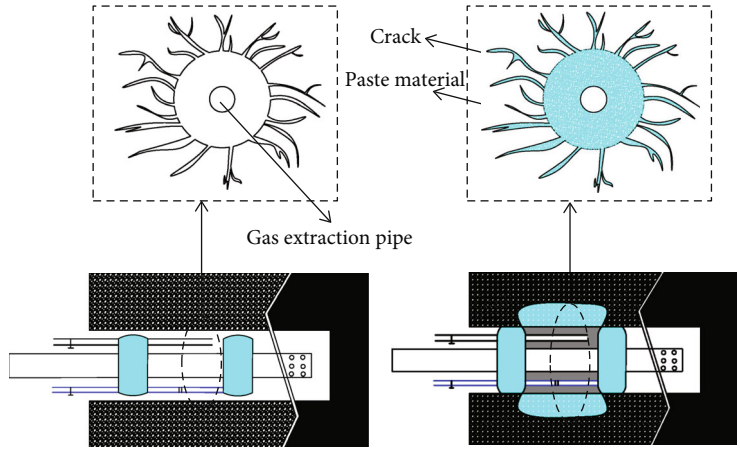

Figure 11: Comparison before and after grouting.

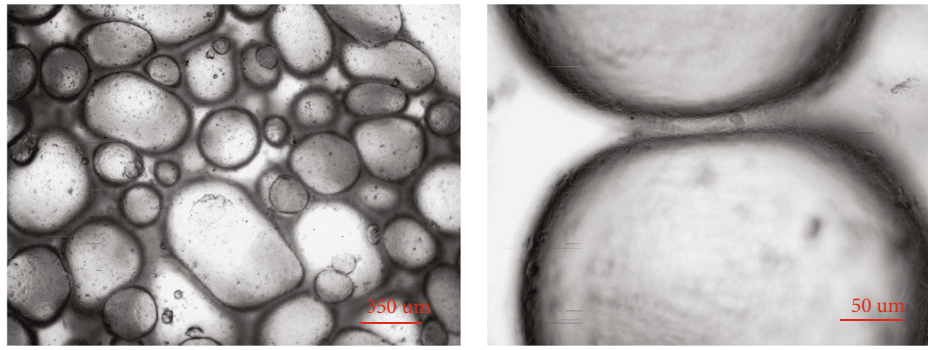

(a) (b)

Figure 12: Optical microstructure of the paste material.

temperature, has good fluidity, can be injected into cracks, and has high compressive strength. At the same time, it improves the utilization rate of phosphogypsum and reduces its pollution to the environment.

A comparison of before and after the borehole wall cracks are filled with the phosphogypsum-based self-produced gas expansion paste material is shown in Figure 11. When the sealing section is full of the paste material, the discharge pipe is closed and the paste material expands and fills the cracks around the borehole wall along the borehole diameter under the effect of the grouting pressure. In the preparation process of the phosphogypsum-based self-produced gas expansion paste material, the addition of polyoxyethylene alkyl and hydroxyethyl cellulose increases the bubble viscosity. Thus, the foam can expand, but the surface is not broken. As shown in Figure 12, the

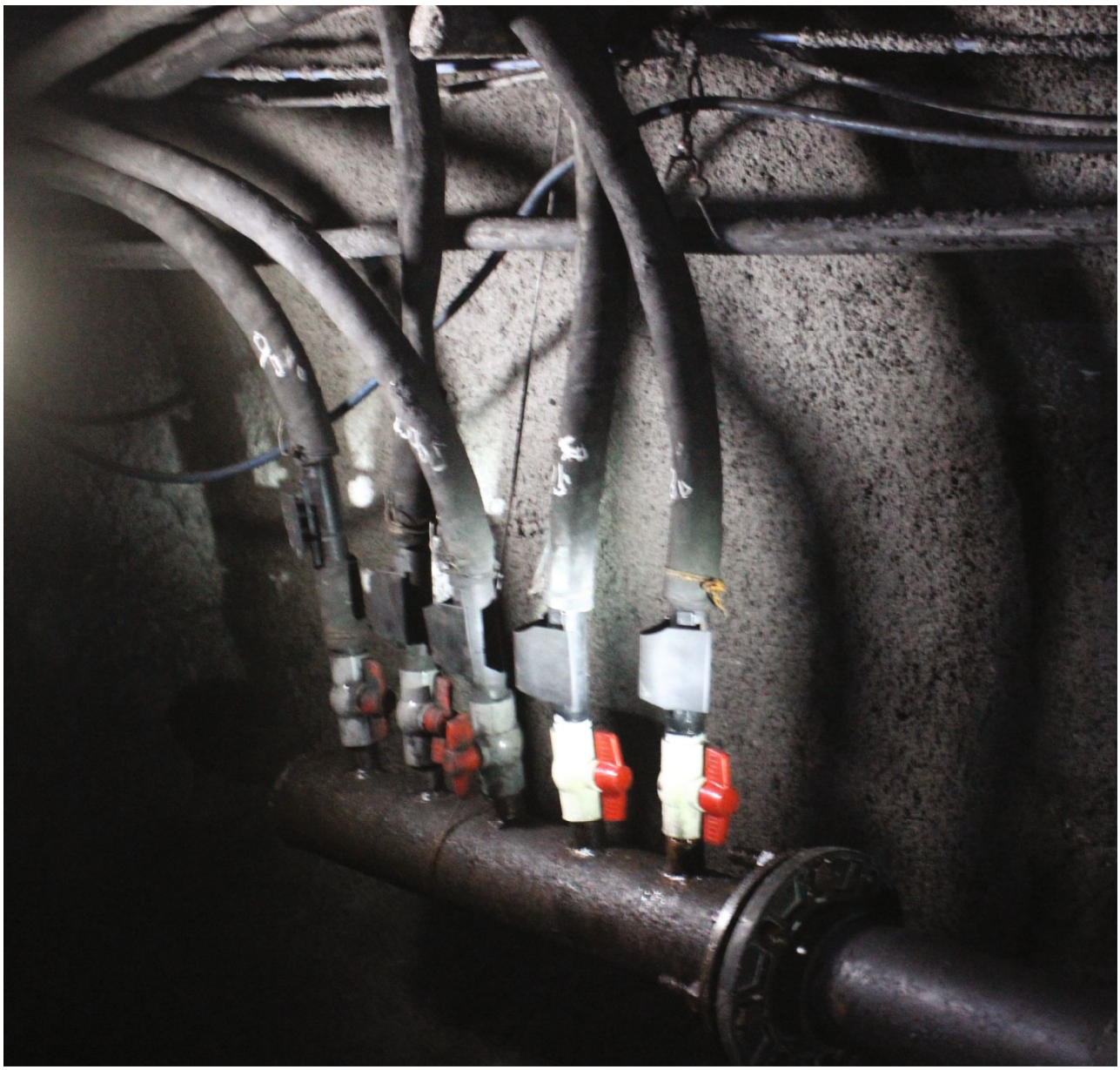

Figure 13: Borehole construction and borehole networking.

foam distribution is homogeneous, and the structure of the foam wall is intact. Therefore, after the paste material enters the cracks, it can effectively seal the cracks and improve the sealing quality. In addition, at normal temperature, the paste material slowly reacts, which ensures good fluidity after the paste material enters into the cracks.

5.3. Result of Test. As shown in Figure 13, the investigation area of each borehole plastic zone was defined as a unit, which was divided into five investigation units, and each unit had five boreholes, and five boreholes of each unit were networked for extraction. The "two blocks and one injection" sealing technology and phosphogypsum-based self-produced gas expansion paste material were used in the test to improve the sealing quality and air tightness. Therefore, accurate data for the gas mixed flow, pure flow,

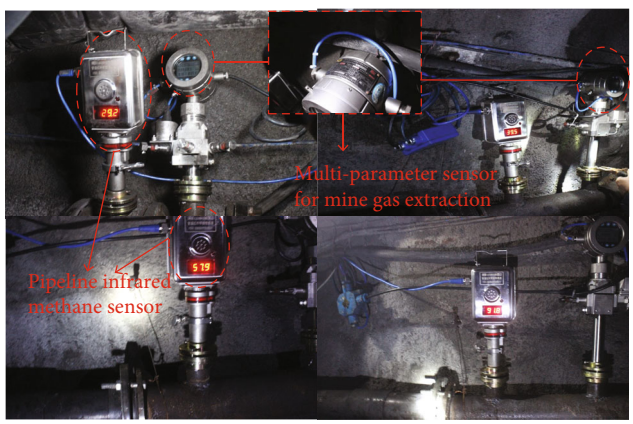

Figure 14: Gas flow concentration.

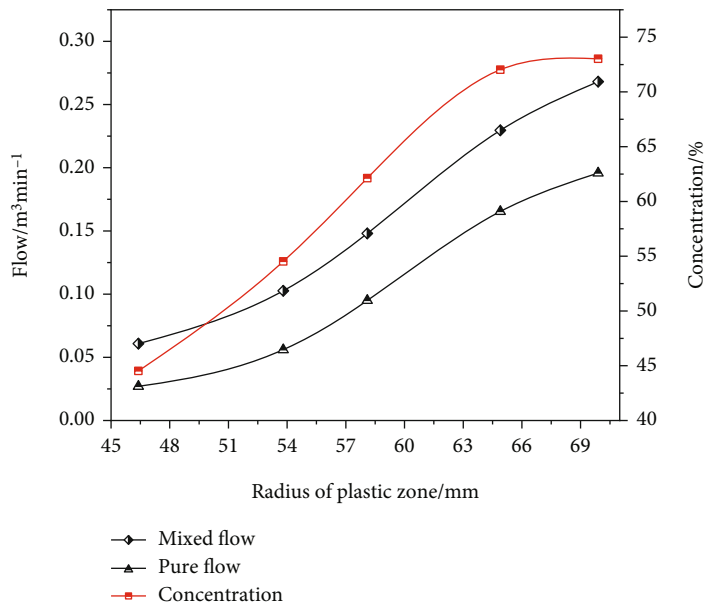

Figure 15: Changes in flow and concentration.

and concentration were measured. After the completion of borehole construction and sealing, the daily gas mixing flow, pure flow, and concentration of each unit were measured for 15 days. The reading on the pipeline infrared methane sensor is the gas concentration of each unit, and the reading on the multiparameter sensor for mine gas extraction is the mixed flow and pure flow of each unit, as shown in Figure 14.

The change rule of the average mixed flow, pure flow, and concentration in the first 15 days of different units is shown in Figure 15. In Figure 15, when the radius of the plastic zone of the borehole increased from 46.4 mm to 69.9 mm, the mixed flow increased from 0.061 m^3/min to 0.268 m^3/min, the pure flow increases from 0.027 m^3/min to 0.196 m^3/min, and the concentration increases from 44.53% to 73.03%. The increased in radius of the plastic zone improved the gas extraction effect.

On one hand, an increase of the plastic zone of the borehole results in an increase of the pressure relief circle around the borehole, which causes a better gas extraction effect. On the other hand, to increase the radius of the plastic zone of the borehole, it is necessary to expand the borehole diameter, which increases construction difficulty, construction cost, and construction risk. Therefore, to achieve safety, cost minimization, and extraction maximization, it is necessary to analyse the variation of the mixed flow and pure flow relative to the radius difference of the plastic zone with the increase of the plastic zone, as shown in Table 5.

As shown in Table 5, the relative variation of mixed flow increased from 5.68 to 21.58 and subsequently decreased to 7.60, while the relative variation of pure flow increased from 3.92 to 18.42 and subsequently decreased to 6.2. With the increased of the radius of the plastic zone, the rates of increased of the mixed flow and pure flow first increased and subsequently decreased. Therefore, considering the safety and economy of construction, the optimal radius of the plastic zone was 64.9 mm.

Table 5: Relative change of the mixed flow and pure flow.

Radius (mm)	Radius difference of plastic (m)	Mixed flow (m^3/min)	Relative variation of mixed flow	Pure flow (m^3/min)	Relative variation of pure flow
46.4 mm	–	0.061	–	0.027	–
53.8 mm	0.0074	0.103	5.68	0.056	3.92
58.1 mm	0.0043	0.148	10.47	0.095	9.07
64.9 mm	0.0038	0.230	12.06	0.165	10.29
69.9 mm	0.005	0.268	7.60	0.196	6.2

6. Conclusions

(1) COMSOL Multiphysics is used to simulate the plastic zone of coal around a borehole. A larger borehole pore corresponds to a larger plastic zone and a larger range of pressure relief of the borehole. The basic model of the plastic zone range is established, and the stress in the elastic zone and radius of the plastic zone are derived step by step. By comparing the radii of the plastic zone from numerical simulation and calculation, the theoretical equation of the radius of the plastic zone is modified. The results show that the modified equation is suitable for Puxi mine

(2) A new type of antispray hole equipment is used to construct a borehole, and the loss and harm caused by borehole spraying are reduced. The "two plugging and one injection" sealing technology and phosphogypsum-based self-produced gas expansion

paste material are used to block the borehole, and the sealing quality is improved

(3) The accurate gas mixing flow, pure flow, and concentration are obtained. With the increase of the plastic zone, the flow of gas extraction gradually increases, but the relative variation of flow first increases and subsequently decreases. Therefore, considering the safety and economy of construction, the optimal radius of the plastic zone is 64.9 mm

Data Availability

The data used to support the findings of this study are included within the article.

Conflicts of Interest

The authors declare no conflict of interest.

Acknowledgments

This work is financially supported by the Hunan Provincial Innovation Foundation For Postgraduate (CX2018B657), the Foundation of Work Safety Key Lab on Prevention and Control of Gas and Roof Disasters for Southern Coal of China (E21825), the National Natural Science Foundation of China (51974299, 51904103, 51974120, and 51974119), the Youth Talent of Hunan Province (2020RC3047), and the Hunan Provincial Natural Science Foundation of China (2019JJ50180 and 2020JJ4023).

References

[1] H. Li, S. L. Shi, B. Q. Lin et al., "Effects of microwave-assisted pyrolysis on the microstructure of bituminous coals," *Energy*, vol. 187, article 115986, 2019.

[2] Q. G. Wang, D. Wang, F. W. Han, F. Yang, and Y. X. Sheng, "Study and application on foam-water mist integrated dust control technology in fully mechanized excavation face," *Process Safety and Environmental Protection*, vol. 133, pp. 41–50, 2020.

[3] Z. L. Xi, X. D. Wang, X. L. Wang et al., "Polymorphic foam clay for inhibiting the spontaneous combustion of coal," *Process Safety and Environmental Protection*, vol. 122, pp. 263–270, 2019.

[4] J. Lin, T. Ren, Y. P. Cheng, J. Nemcik, and G. D. Wang, "Cyclic N2 injection for enhanced coal seam gas recovery: a laboratory study," *Energy*, vol. 188, article 116115, 2019.

[5] Y. Lu, S. L. Shi, H. Q. Wang, Z. J. Tian, Q. Ye, and H. Y. Niu, "Thermal characteristics of cement microparticle-stabilized aqueous foam for sealing high-temperature mining fractures," *International Journal of Heat and Mass Transfer*, vol. 131, pp. 594–603, 2019.

[6] Q. Ye, G. X. Wang, Z. Z. Jia, and C. S. Zheng, "Experimental study on the influence of wall heat effect on gas explosion and its propagation," *Applied Thermal Engineering*, vol. 118, pp. 392–397, 2017.

[7] Y. Lu, "Laboratory study on the rising temperature of spontaneous combustion in coal stockpiles and a paste foam suppression technique," *Energy & Fuels*, vol. 31, no. 7, pp. 7290–7298, 2017.

[8] Z. Z. Zhang, M. Deng, J. B. Bai, X. Y. Yu, Q. H. Wu, and L. S. Jiang, "Strain energy evolution and conversion under triaxial unloading confining pressure tests due to gob-side entry retained," *International Journal of Rock Mechanics and Mining Sciences*, vol. 126, article 104184, 2020.

[9] Q. Ye, Z. Z. Jia, and C. S. Zheng, "Study on hydraulic-controlled blasting technology for pressure relief and permeability improvement in a deep hole," *Journal of Petroleum Science and Engineering*, vol. 159, pp. 433–442, 2017.

[10] G. F. Li, H. A. Zheng, and D. S. Fu, "Research progress of polyurethane for coal mining borehole sealing engineering," *Clean Coal Technology*, vol. 20, pp. 94–98, 2014.

[11] Q. G. Li, B. Q. Lin, and C. Zhai, "The effect of pulse frequency on the fracture extension during hydraulic fracturing," *Journal of Natural Gas Science and Engineering*, vol. 21, pp. 296–303, 2014.

[12] C. J. Wang, S. Q. Yang, and X. W. Li, "Simulation of the hazard arising from the coupling of gas explosions and spontaneously combustible coal due to the gas drainage of a gob," *Process Safety and Environmental Protection*, vol. 118, pp. 296–306, 2018.

[13] K. Noack, "Control of gas emissions in underground coal mines," *International Journal of Coal Geology*, vol. 35, no. 1-4, pp. 57–82, 1998.

[14] X. L. Zhang, B. Q. Lin, C. Zhu et al., "Petrophysical variation of coal treated by cyclic high-voltage electrical pulse for coalbed methane recovery," *Journal of Petroleum Science and Engineering*, vol. 178, pp. 795–804, 2019.

[15] G. H. Ni, H. C. Xie, Z. Li, and Y. Y. Niu, "Improving the permeability of coal seam with pulsating hydraulic fracturing technique: a case study in Changping coal mine, China," *Process Safety and Environmental Protection*, vol. 117, pp. 565–572, 2018.

[16] C. Karacan, F. A. Ruiz, M. Cotè, and S. Phipps, "Coal mine methane: a review of capture and utilization practices with benefits to mining safety and to greenhouse gas reduction," *International Journal of Coal Geology*, vol. 86, no. 2-3, pp. 121–156, 2011.

[17] M. Pillalamarry, S. Harpalani, and S. M. Liu, "Gas diffusion behavior of coal and its impact on production from coalbed methane reservoirs," *International Journal of Coal Geology*, vol. 86, no. 4, pp. 342–348, 2011.

[18] H. Zhang, Y. P. Cheng, Q. Q. Liu et al., "A novel in-seam borehole hydraulic flushing gas extraction technology in the heading face: enhanced permeability mechanism, gas flow characteristics, and application," *Journal of Natural Gas Science and Engineering*, vol. 46, pp. 498–514, 2017.

[19] J. Dong, Y. P. Cheng, K. Jin et al., "Effects of diffusion and suction negative pressure on coalbed methane extraction and a new measure to increase the methane utilization rate," *Fuel*, vol. 197, pp. 70–81, 2017.

[20] L. Qin, C. Zhai, J. Z. Xu, S. M. Liu, C. Zhong, and G. Q. Yu, "Evolution of the pore structure in coal subjected to freeze –thaw using liquid nitrogen to enhance coalbed methane extraction," *Journal of Petroleum Science and Engineering*, vol. 175, pp. 129–139, 2019.

[21] C. M. Shen, B. Q. Lin, C. Sun, Q. Z. Zhang, and Q. Z. Li, "Analysis of the stress-permeability coupling property in water jet slotting coal and its impact on methane drainage," *Journal of*

Petroleum Science and Engineering, vol. 126, pp. 231–241, 2015.

[22] B. B. Li, K. Yang, P. Xu, J. Xu, M. Yuan, and M. Zhang, "An experimental study on permeability characteristics of coal with slippage and temperature effects," *Journal of Petroleum Science and Engineering*, vol. 175, pp. 294–302, 2019.

[23] B. Q. Lin, H. R. Song, Y. Zhao, T. Liu, J. Kong, and Z. B. Huang, "Significance of gas flow in anisotropic coal seams to underground gas drainage," *Journal of Petroleum Science and Engineering*, vol. 180, pp. 808–819, 2019.

[24] C. Karacan, W. Diamond, and S. Schatzel, "Numerical analysis of the influence of in-seam horizontal methane drainage boreholes on longwall face emission rates," *International Journal of Coal Geology*, vol. 72, no. 1, pp. 15–32, 2007.

[25] X. F. Liu, D. Z. Song, X. Q. He, Z. P. Wang, M. R. Zeng, and K. Deng, "Nanopore structure of deep-burial coals explored by AFM," *Fuel*, vol. 246, pp. 9–17, 2019.

[26] M. R. Islam, D. Hayashi, and A. Kamruzzaman, "Finite element modeling of stress distributions and problems for multi-slice longwall mining in Bangladesh, with special reference to the Barapukuria coal mine," *International Journal of Coal Geology*, vol. 78, no. 2, pp. 91–109, 2009.

[27] Y. F. Zhang, S. Y. Hu, T. Q. Xia, Y. K. Liu, Z. Pan, and F. B. Zhou, "A novel failure control technology of cross-measure borehole for gas drainage: a case study," *Process Safety and Environmental Protection*, vol. 135, pp. 144–156, 2020.

[28] Y. Niu, Z. H. Li, E. Y. Wang et al., "Study on characteristics of EP responsing to coal mining," *Engineering Fracture Mechanics*, vol. 224, article 106780, 2020.

[29] Y. Niu, X. Y. Song, Z. H. Li et al., "Experimental study and field verification of stability monitoring of gas drainage borehole in mining coal seam," *Journal of Petroleum Science and Engineering*, vol. 189, article 106985, 2020.

[30] L. D. Guo, X. S. Zhao, and Y. J. Zhang, "Study on borehole sealing technique with sealing and isolation integration to gas drainage borehole along seam," *Coal Science and Technology*, vol. 46, no. 5, pp. 114–119, 2018.

[31] H. M. Cheng, Y. D. Qiao, and C. L. Dong, "Study on hydraulic fractured gas drainage effect based on Hoek-Brown criterion," *Coal Science and Technology*, vol. 46, no. 9, pp. 111–116, 2018.

[32] G. P. Su, "Pressure relief range and stress distribution of coal body around borehole for gas extraction along seam," *China Energy and Environmental Protection*, vol. 41, no. 10, pp. 21–24, 2019.

[33] H. Frank, R. Ting, and A. Naj, "Evolution and application of in-seam drilling for gas drainage," *International Journal of Mining Science and Technology*, vol. 23, no. 4, pp. 543–553, 2013.

[34] C. S. Zheng, B. Y. Jiang, S. Xue, Z. W. Chen, and H. Li, "Coalbed methane emissions and drainage methods in underground mining for mining safety and environmental benefits: a review," *Process Safety and Environmental Protection*, vol. 127, pp. 103–124, 2019.

[35] C. Zhang, B. Q. Lin, Y. Zhou, C. Zhai, and C. J. Zhu, "Study on "fracturing-sealing" integration technology based on high-energy gas fracturing in single seam with high gas and low air permeability," *International Journal of Mining Science and Technology*, vol. 23, no. 6, pp. 841–846, 2013.

[36] C. Zhang, B. Q. Lin, and Y. Zhou, "Strong-weak-strong borehole pressurized sealing technology for horizontal gas drainage borehole in mining seam," *Journal of Mining and Safety Engineering*, vol. 30, pp. 935–939, 2013.

[37] Q. Q. Liu, Y. P. Cheng, L. Yuan, Y. X. Fang, D. Z. Shi, and S. L. Kong, "A new effective method and new materials for high sealing performance of cross-measure CMM drainage boreholes," *Journal of Natural Gas Science and Engineering*, vol. 21, pp. 805–813, 2014.

[38] F. B. Zhou, J. H. Li, X. Ze, Y. K. Liu, R. G. Zhang, and S. J. Shen, "A study of the second hole sealing method to improve gas drainage in coal seams," *Journal of China University of Mining & Technology*, vol. 38, pp. 764–768, 2009.

[39] G. H. Ni, B. Q. Lin, and C. Zhai, "Microscopic properties of drilling sealing materials and their influence on the sealing performance of boreholes," *Journal of University of Science and Technology Beijing*, vol. 35, pp. 572–579, 2013.

[40] X. W. Xiang, C. Zhai, Y. M. Xu, X. Yu, and J. Z. Xu, "A flexible gel sealing material and a novel active sealing method for coalbed methane drainage boreholes," *Journal of Natural Gas Science and Engineering*, vol. 26, pp. 1187–1199, 2015.

[41] Z. L. Ge, X. D. Mei, and Y. Y. Lu, "Mechanical model and test study of sealed drilling for hydraulic fracturing in underground coal mines," *Journal of Basic Science and Engineering*, vol. 22, pp. 1128–1139, 2014.

[42] L. Qin, P. Wang, S. G. Li et al., "Gas adsorption capacity changes in coals of different ranks after liquid nitrogen freezing," *Fuel*, vol. 292, article 120404, 2021.

[43] L. Qin, P. Wang, S. G. Li et al., "Gas adsorption capacity of coal frozen with liquid nitrogen and variations in the proportions of the organic functional groups on the coal after freezing," *Energy Fuels*, vol. 35, no. 2, pp. 1404–1413, 2021.

[44] H. Li, L. Tian, B. X. Huang et al., "Experimental study on coal damage subjected to microwave heating," *Rock Mechanics and Rock Engineering*, vol. 53, no. 12, pp. 5631–5640, 2020.

[45] J. X. Lu, H. Li, S. L. Shi et al., "Microwave-induced microstructure evolution of coal and its effects on the methane adsorption characteristic," *Energy Fuels*, vol. 35, no. 5, pp. 4081–4090, 2021.